MRI-based Pseudo-CT Generation Using Sorted Atlas Images in Whole-body PET/MRI

Hossein Arabi and Habib Zaidi†, *Senior Member, IEEE*

***Abstract*– In this work, we propose a novel approach for MRI-based generation of pseudo-CT images in whole-body PET/MRI based on Hofmann's pattern recognition and atlas registration approach. The major improvement emanates from sorting registered atlas images based on voxelwise local normalized cross-correlation and choosing the most similar atlas image for Gaussian process regression (GPR) analysis. Furthermore, prior knowledge derived from the correlation between lung volume and attenuation coefficients was embedded in the GPR kernel for accurate patient-specific prediction of lung attenuation coefficients. Modifying the GPR algorithm improved the similarity index of bone extraction from 0.55 to 0.61 and enabled significant bias reduction of tracer uptake (SUV) in bony regions. Incorporating prior knowledge about lung volume in the GPR algorithm resulted in SUV_{mean} bias reduction from 8.9% to 4.1% in the whole lung region. Overall, the proposed algorithm provided more accurate PET quantification in the lungs and bony regions.**

I. Introduction

The quantitative capabilities of PET/MRI need to be improved and validated to enable the realization of the full potential of this hybrid technology in clinical and research setting [1]. The aim of this study is to present a novel MRI-based attenuation correction approach in whole-body PET/MRI. This approach builds on Hofmann's algorithm [2] to add additional prior information enabling improved performance. To this end, MR images of 14 patients are non-rigidly registered to target MR image. The obtained transformation fields are then used to warp the corresponding CT images. Local normalized cross-correlation is employed to find the most similar image in the atlas data set for each voxel. Gaussian process regression is then performed on the selected atlas. Moreover, the variability of lung attenuation coefficients across patients, prior knowledge derived from the correlation between lung attenuation coefficients and lung volume was incorporated in the regression process to estimate more accurately patient-specific lung attenuation coefficients.

II. Material and Methods

A. Data preparation

The acquired MR images contain a relatively high level of noise, corruption due to the low frequency bias field and inter-patient intensity inhomogeneity [3]. As such, the presence of any aforementioned source of intensity uncertainty in MR images might bias the pseudo-CT generation result. To overcome these prospective sources of error, in-phase images of all patients underwent the following pre-processing steps.

Gradient anisotropic diffusion filtering using the following parameters: conductance = 4, number of iterations = 10 and time step = 0.01. This is an edge preserving smoothing algorithm that adjusts the conductance term to produce large diffusion inside regions where the gradient magnitude is relatively small (homogenous regions) and lesser diffusion in regions where the gradient magnitude is large (i.e. edges).

N4 bias field correction [4]: B-spline grid resolution = 400, number of iterations = 200 (at each grid resolution), convergence threshold = 0.001, B-spline order = 3, spline distance = 400, number of histogram bins = 256 and shrink factor = 3.

Histogram matching [5]: Histogram level = 512 and match points = 64. In order to get the best result from histogram matching, it is recommended to exclude background air voxels of both reference and target images before processing.

Normalization to the average water intensity: To overcome inter-patient MR intensity non-uniformity, in addition to histogram matching, each in-phase image was normalized to the average intensity of the corresponding water image. To this end, fuzzy C-means clustering [6] was employed to segment Dixon water-only images into 3 distinct classes. The obtained mask of the third class on water-only image was used to calculate the mean intensity of the corresponding in-phase image. The latter was then used to normalize the in-phase image.

The external body contour was determined by applying a 3D snake active contour algorithm on the in-phase MR images [7]. Identification and segmentation of the lungs was performed through connected-component analysis of the lower intensity in the inner part of the body using the ITK-SNAP image processing software [8].

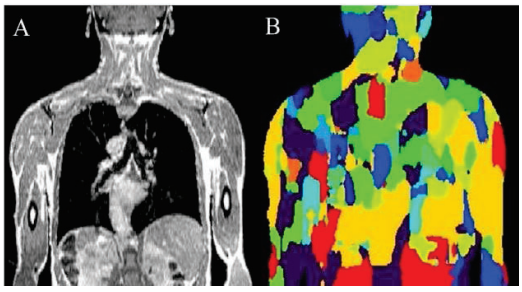

Fig 1. (A) Dixon image of the target patient. (B) Atlas-selection matrix where each color corresponds to one image in the atlas data set.

We used a leave-one-out cross-validation (LOOCV) approach, that for each individual patient all the remaining thirteen in-phase MR images were deformably registered to the

H. Arabi is with the Division of Nuclear Medicine & Molecular Imaging, Geneva University Hospital, CH-1211, Geneva, Switzerland (e-mail: hossein.arabi@etu.unige.ch).

†H. Zaidi is with the Division of Nuclear Medicine and Molecular Imaging, Geneva University Hospital, CH-1211 Geneva, Switzerland, Geneva, Neuroscience Center, Geneva University, CH-1205 Geneva, Switzerland, and Department of Nuclear Medicine and Molecular Imaging, University of Groningen, University Medical Center Groningen, Groningen, Netherlands (e-mail: habib.zaidi@hcuge.ch).

978-1-4799-6097-2/14/$31.00 ©2014 IEEE

target image using the Elastix package [9]. The alignment was performed by employing a combination of rigid registration based on maximum mutual information and non-rigid registration as described previously [10].

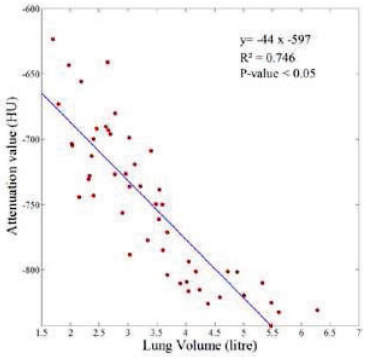

Fig.2. Correlation between lung volume and lung attenuation coefficients.

B. Gaussian Regression Process

Hofmann's approach [2] uses the Gaussian covariance kernel function where W is a weighing factor for patches defined on MR images (P_{MR}), X is the voxel position and P_{seg} is the patch from 5-class segmented MRI.

$$K(d_i,d_j)=\exp\left(\frac{-\left\|w(P_{MR,i})-\ w(P_{MR,j})\right\|^2}{2\sigma^2_{MR,patch}}\right)\times\ \exp\left(\frac{-\|X_i-X_j\|^2}{2\sigma^2_{pos}}\right)\times\exp\left(\frac{-\|W(P_{Seg,i})-W(P_{Seg,j})\|^2}{2\sigma^2_{Seg,patch}}\right) \quad (1)$$

In the proposed approach, the Gaussian kernel (Eq. 1) is divided into two separate kernels, one for non-lung tissues (Eq. 2) and one for lung tissues (Eq. 5). In the non-lung kernel, instead of rectangular patches on MR (P_{MR}) and segmented MR (P_{seg}), only the voxel value (MR_C) in the clustered MR image obtained by K-mean + Markov random field is used, while the term related to the position remains intact.

$$K_{non-lung}(b_i,b_j)=\exp\left(\frac{-\|MR_{C,i}-MR_{C,j}\|^2}{2\sigma^2_{MR,cluster}}\right)\times\ \exp\left(\frac{-\|X_i-X_j\|^2}{2\sigma^2_{pos}}\right) \quad (2)$$

In the next step, all the registered MR images are compared voxelwise to the target MR image using local normalized cross correlation algorithm (Eq. 3). Since this algorithm is markedly sensitive to noise when it comes to voxel level, the k-nearest neighbour criterion (Eq. 4) was utilized to determine the most similar atlas to that voxel of the target image. The result is called atlas-selection matrix *R(x)* (Fig. 1), where each color corresponds to a single image in the atlas data set. Subsequently, the learning process and pseudo-CT generation (Eq. 2) is performed through most similar image in atlas data set for each voxel.

$$LNCC_v=\frac{\langle Im,Iref\rangle_v}{\sigma(Im)_v\,.\,\sigma(Iref)_v} \quad (3)$$

$$\langle Im,Iref\rangle_v=(K_G\otimes Im.Iref)-((K_G\otimes Im)\,.\,(K_G\otimes Iref))$$

$$\sigma(Im)_v=\sqrt{(K_G\otimes Im^2)-(K_G\otimes Im)^2}$$

$$K_G=\ \mathcal{N}(\mu,\sigma^2)$$

$$R(x)=\left|\left\{i:\sum_k LNCC_i>\sum_k LNCC_j\right\}\right| \quad (4)$$

It was noticed that there is a correlation between lung volume and its attenuation coefficient (Fig. 2). In this light, the term considering the volume of lung (V) was embedded in Gaussian process regression to estimate the lung attenuation coefficient more accurate and patient-specific.

$$K_{lung}(l_i,l_j)=\exp\left(\frac{-\|MR_{c,i}-MR_{c,j}\|^2}{2\sigma^2_{MR,cluster}}\right)\times exp\left(\frac{-\|V_i-V_j\|^2}{2\sigma^2_{Lung\ volume}}\right) \quad (5)$$

C. Quantitative evaluation

The quantitative accuracy of the proposed approach was assessed using 14 clinical studies of patients, who underwent whole body ^{18}F-FDG PET/MR and PET/CT for staging of head and neck malignancies. PET images were reconstructed using the e7 tool (Siemens Healthcare, Knoxville, TN) using attenuation weighted, ordered subset-expectation maximization (AW-OSEM) iterative reconstruction algorithm using default parameters (4 iterations, 8 subsets, and a post-processing Gaussian kernel with a FWHM of 5 mm) adopted on the multimodality workstation (Siemens Healthcare, Hoffman Estates, IL, USA). Image reconstruction was performed four times for each clinical study: PET images corrected for attenuation using CT (PET-CTAC) used as reference, using the 3-class attenuation map (PET-MRAC3c) [11] obtained from the Ingenuity TF PET/MR scanner (Philips Healthcare) [12], using the pseudo-CT generated by Hofmann's approach (PET-HofmannAC) [2] and our proposed SAP (sorted atlas selection) approach (PET-SAPAC). A nuclear medicine physician drew manually the VOIs on regions of normal physiologic uptake, six regions in the lungs, liver, spleen, cerebellum, 2 bony structures (cervical vertebrae 6 and dorsal vertebrae 5), aorta, and malignant lesions. The differences between the attenuation correction techniques were quantified in terms of change in the standard uptake value (SUV). The SUVs were calculated by dividing the activity concentration in each VOI by the injected activity divided by body weight.

The assessment of the accuracy and robustness of extracted bones using the proposed (SAP) and Hofmann's approaches was performed through comparison with the bone segmented from the corresponding CT images. Bone segmentation was performed by applying a threshold of 180 HUs on the generated pseudo-CT and corresponding CT images. The validation of bone segmentation is reported using five volume/distance-based metrics: Dice similarity (DSC) [13], relative volume difference (RVD), Jaccard similarity (JC), sensitivity (S) and mean absolute surface distance (MASD).

$$DSC(A,M)=\frac{2|A\cap M|}{|A|+|M|} \qquad RVD(A,M)=100\times\frac{|A|-|M|}{|M|}$$

$$JC(A,M)=\frac{|A\cap M|}{|A\cup M|} \qquad S(A,M)=\frac{|A\cap M|}{|M|}$$

$$MASD(A,M)=\frac{d_{ave}\ (S_A,A_M)+d_{ave}\ (A_M,S_A)}{2}$$

where A is the bone segmented from the reference CT image and M denotes the extracted bone from the pseudo-CT attenuation maps. $D_{ave}(S_A,S_M)$ is the average direct surface distance from all points on the CT bone surface S_A and to the pseudo-CT bone surface S_M.

The accuracy of the predicted lung attenuation coefficient was evaluated by calculating the average lung attenuation coefficient on the obtained pseudo-CT images using a lung mask and comparing it with the corresponding CT images for each individual patient. Shapiro-Wilk test was used to examine the null hypothesis that the estimates follow a normally distributed population and the obtained results were considered statistically significant if the p-value was less than 0.05.

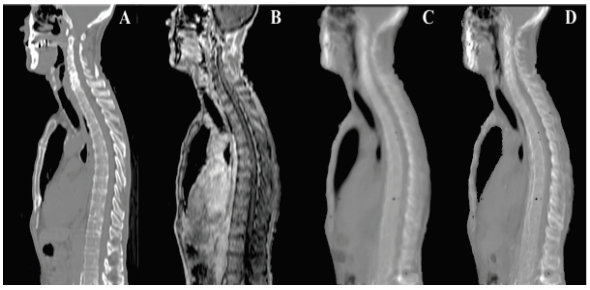

Fig.3. A: Corresponding CT image. B: Target MR image. C: Pseudo-CT Hofmann approach D: Pseudo-CT obtained from SAP approach.

III. Results

Fig. 3 depicts the pseudo-CT images generated using Hofmann's and our proposed approach. The mean similarity index calculated for extracted bone on the basis of 14 patients is 0.58±0.09 and 0.65±0.07, respectively (table 1). The representative extracted bone slices from Hofmann's approach pseudo CT and the new proposed method is illustrated in Fig. 4 along with reference CT image and distance error map. This improvement is due to the sorting the registered atlas data set based on local normalized cross-correlation that resulted in more patient specific pseudo-CT. Incorporating the prior knowledge of the lung volume in the regression process rendered the estimated attenuation coefficients of the lungs for each patient closer to the reference (CT) (Fig. 5). It can be concluded that the proposed method is more accurate than averaging lung attenuation values over the whole atlas data set. The more accurate SUV_{mean} estimates demonstrate the improvement of attenuation map in bony regions and cerebellum and patient-specific derivation of lung attenuation coefficients with considerable lower standard deviation (Fig. 6). The mean SUV bias in the whole lung region decreased from 8.9% to 4.1%.

Table 1. Comparison of validation measures (mean±SD), Dice similarity (DSC), relative volume distance (RVD), Jaccard similarity (JC), Sensitivity (S) and mean absolute surface distance (MASD) between the bone extracted from Hofmann's and proposed attenuation maps.

	Hofmann	SAP
DSC	0.58 ± 0.09	0.65 ±0.07
RVD (%)	-36.6 ± 10.0	-30.7 ± 09.1
JC	0.35 ± 0.06	0.41 ±0.05
S	0.40 ± 0.15	0.48 ± 0.12
MASD (mm)	6.92 ± 3.1	4.81 ± 2.6

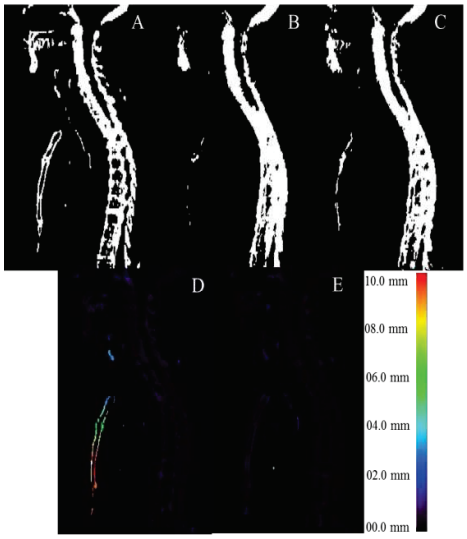

Fig 4. Representative slice of bone segmentation from MR image. A) Binary image of segmented bone from CT image B) segmented bone obtain from Hofmann pseudo-CT generation algorithm C) Segmented bone utilizing the new method D) Distance error map calculated from comparison of Hofmann pseudo-CT and E) new approach with the reference bone segmented on the CT image.

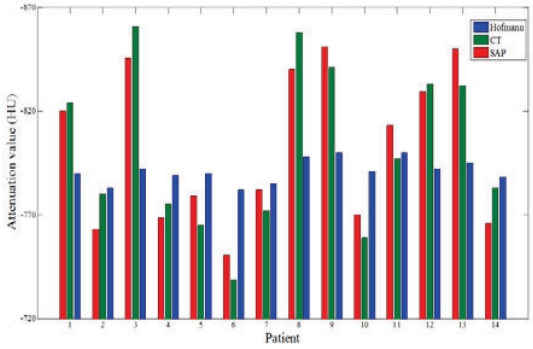

Fig. 5. 14 patients lung attenuation coefficients obtained using the new approach (SAP) compared to Hofmann's approach and the reference (CT).

IV. Conclusion

We proposed a new whole-body pseudo-CT generation approach exploiting the concept of co-registered atlas and pattern recognition. The SAP technique improved bone extraction leading to more accurate SUV estimation, particularly in bony structures and lung regions even in the presence of malignant abnormalities. Future work will focus on further improvement of bone extraction accuracy through optimization of atlas fusion and reduction of the computational time needed for atlas registration through alignment of multiple atlas images using a single registration to render the technique practical for clinical usage.

V. Acknowledgments

This work was supported by the Swiss National Science Foundation under grant SNSF 31003A-149957.

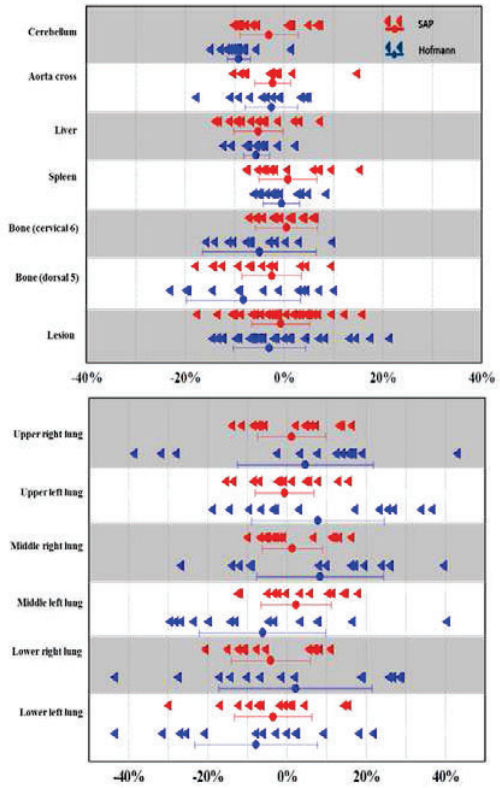

Fig. 6. Mean SUV uptake in different regions on the basis of Hofmann's and new pseudo-CT attenuation map.

REFERENCES

[1] H. Zaidi and A. Del Guerra, "An outlook on future design of hybrid PET/MRI systems.," *Med Phys,* vol. 38, pp. 5667-5689, 2011.

[2] M. Hofmann, I. Bezrukov, F. Mantlik, P. Aschoff, F. Steinke, T. Beyer*, et al.*, "MRI-based attenuation correction for whole-body PET/MRI: Quantitative evaluation of segmentation- and Atlas-based methods.," *J Nucl Med,* vol. 52, pp. 1392-1399, 2011.

[3] J. M. Lotjonen, R. Wolz, J. R. Koikkalainen, L. Thurfjell, G. Waldemar, H. Soininen*, et al.*, "Fast and robust multi-atlas segmentation of brain magnetic resonance images.," *Neuroimage,* vol. 49, pp. 2352-2365, 2010.

[4] N. J. Tustison, B. B. Avants, P. A. Cook, Y. Zheng, A. Egan, P. A. Yushkevich*, et al.*, "N4ITK: improved N3 bias correction.," *IEEE Trans Med Imaging,* vol. 29, pp. 1310-1320, 2010.

[5] M. J. McAuliffe, F. M. Lalonde, D. McGarry, W. Gandler, K. Csaky, and B. L. Trus, "Medical Image Processing, Analysis and Visualization in clinical research," in *14th IEEE Symposium on Computer-Based Medical Systems, 2001. CBMS 2001. Proceedings*, 2001, pp. 381-386.

[6] J. C. Bezdek, *Pattern Recognition with Fuzzy Objective Function Algorithms*. Norwell, MA, USA: Kluwer Academic Publishers, 1981.

[7] M. Kass, A. Witkin, and D. Terzopoulos, "Snakes: active contour models.," *Int J Comput Vision,* vol. 1, pp. 321-331, 1988.

[8] P. A. Yushkevich, J. Piven, H. C. Hazlett, R. G. Smith, S. Ho, J. C. Gee*, et al.*, "User-guided 3D active contour segmentation of anatomical structures: significantly improved efficiency and reliability.," *Neuroimage,* vol. 31, pp. 1116-1128, 2006.

[9] S. Klein, M. Staring, K. Murphy, M. A. Viergever, and J. P. W. Pluim, "elastix: A toolbox for intensity-based medical image registration.," *IEEE Trans Med Imaging,* vol. 29, pp. 196-205, 2010.

[10] A. Akbarzadeh, D. Gutierrez, A. Baskin, M. R. Ay, A. Ahmadian, N. Riahi Alam*, et al.*, "Evaluation of whole-body MR to CT deformable image registration.," *J Appl Clin Med Phys,* vol. 14, pp. 238-253, 2013.

[11] V. Schulz, I. Torres-Espallardo, S. Renisch, Z. Hu, N. Ojha, P. Börnert*, et al.*, "Automatic, three-segment, MR-based attenuation correction for whole-body PET/MR data.," *Eur J Nucl Med Mol Imaging,* vol. 38, pp. 138-152, 2011.

[12] H. Zaidi, N. Ojha, M. Morich, J. Griesmer, Z. Hu, P. Maniawski*, et al.*, "Design and performance evaluation of a whole-body Ingenuity TF PET-MRI system.," *Phys Med Biol,* vol. 56, pp. 3091-3106, 2011.

[13] L. R. Dice, "Measures of the amount of ecologic association between species.," *Ecology,* vol. 26, pp. 297-302, 1945.